Applied Surface Science 559 (2021) 149463

Contents lists available at ScienceDirect

Applied Surface Science

journal homepage: www.elsevier.com/locate/apsusc

Full Length Article

Thermal transport property of novel two-dimensional nitride phosphorus: An ab initio study

Bing Lv [a,b], Xiaona Hu [c], Ning Wang [d], Jia Song [e], Xuefei Liu [a,b], Zhibin Gao [f,*]

[a] School of Physics and Electronic Science, Guizhou Normal University, Guiyang 550025, China
[b] Key Laboratory of Low Dimensional Condensed Matter Physics of Higher Educational Institution of Guizhou Province, Guizhou Normal University, Guiyang 550025, China
[c] School of Biological Sciences, Guizhou Education University, Guiyang 550018, China
[d] School of Physics, University of Electronic Science and Technology of China, Chengdu 610054, China
[e] Shanghai Engineering Research Center of 3D Printing Materials, Shanghai Research Institute of Materials, Shanghai 200437, China
[f] State Key Laboratory for Mechanical Behavior of Materials, Xi'an Jiaotong University, Xi'an 710049, China

ARTICLE INFO

Keywords:
First-principles calculation
Phonon anharmonicity
Thermal transport
2D nitride phosphorus (NP)

ABSTRACT

Controlling thermal transport property is a crucial issue toward thermal management in two-dimensional (2D) materials. With first-principles calculations and Boltzmann transport equation (BTE), we have explored the thermal transport property of novel 2D nitride phosphorus (NP). We find that, at room temperature, the calculated lattice thermal conductivity (κ_{lat}) of novel 2D NP is 25.4 W/mK, being lower than that of buckled monolayer phosphorene, nitrogene, and β-NP. Through the analysis of corresponding phonon–phonon scattering channels (a + a ↔ o and a + o ↔ o), we find that the strong scatterings among acoustic phonons and low-frequency optical phonons are accountable for the low κ_{lat} of novel 2D NP. Additionally, we also study the sample size effects of novel 2D NP, which can further decrease κ_{lat} until a length of up to 5 μm. These results could provide valuable guidance to design the NP-based thermoelectric nano-devices and potential heat transport applications in other 2D materials.

1. Introduction

The widespread concern has been paid to thermoelectric technology, which can generate electricity from waste heat [1,2]. The thermoelectric efficiency is decided by the thermoelectric (TE) figure of merit (ZT), which is computed as $S^2\sigma T/(\kappa_e + \kappa_{lat})$. The meanings of these parameters are extensively explained elsewhere [3]. For one TE material, a high-power factor ($S^2\sigma$) and a low κ_{lat} are required for obtaining excellent performance, while those TE transport coefficients are strongly coupled to each other. Apart from the contradictory relation between S and σ [3], there is also a conflict between σ and κ_e [4,5]. Therefore, it is a great challenge to obtain a high ZT value by modifying those coefficients simultaneously. Among them, the κ_{lat} is a very interesting parameter, which can be adjusted independently to improve the ZT value since phonons mean-free-path is much smaller than that of electrons. Hence, it is of great significance to search out an ideal TE material with low lattice thermal conductivity.

During the last few years, the stable binary compounds of group VA have attracted wide attention [6–9]. For example, the κ_{lat} of 10.97 W/mK for monolayer α-AsP is lower than that of 29.95 W/mK for the single element monolayer α-P [8]. Similarly, Sevik *et al.* proved that the κ_{lat} of α-P, α-As and α-Sb monolayers might be suppressed by alloying with the group VA elements as well, and κ_{lat} of α-PBi along the armchair direction was predicted to be as low as 1.5 W/mK, whereas that of α-P was 21 W/mK [7]. Besides, compared with the κ_{lat} of 46.6 W/K and 161.1 W/K for Sb and As monolayers, lower κ_{lat} of 28.8 W/K the monolayer β-SbAs was also reported [6]. Recently, the κ_{lat} of β-NX (X = P, As, Sb) monolayers were investigated by Taheri et al.[9]. The results showed that β-NP possesses the smallest κ_{lat} of 572.3 W/K compared with β-NAs and β-NSb monolayers. However, the κ_{lat} of those binary compounds are higher than those of the corresponding monolayer β-P, β-As, and β-Sb, which are obviously different from monolayer α-AsP and β-SbAs. The turn-around is that, in 2019, Zhu *et al.* proposed a new 2D material SnSe with ultra-low κ_{lat} and excellent thermoelectric performance [10]. This evidence motivates us to check whether the structure of novel 2D NP as SnSe-like isoelectronic counterpart material is stable or not? Besides, we

* Corresponding author at: State Key Laboratory for Mechanical Behavior of Materials, Xi'an Jiaotong University, Xi'an 710049, China.
E-mail address: zhibin.gao@xjtu.edu.cn (Z. Gao).

https://doi.org/10.1016/j.apsusc.2021.149463
Received 29 October 2020; Received in revised form 31 January 2021; Accepted 1 March 2021
Available online 4 March 2021

are deserved to investigate the answer that whether the κ_{lat} of novel 2D NP is lower than that of β-NP or not?

Inspired by these integrated and interesting questions, here, we focus on the κ_{lat} of novel 2D NP based on the phonon Peierls-Boltzmann equation. Our calculations show that, at room temperature, the novel 2D NP exists a low κ_{lat} of 25.4 W/mK, which is smaller than those of buckled monolayer phosphorene(108.8 W/mK [11]), nitrogene (763.4 W/mK [12]), and β-NP (572.3 W/K [9]). Such a low κ_{lat} in novel 2D NP largely attributes to the stronger scattering rates of a + a ↔ o and a + o ↔ o channels, which is derived from the strong scattering interactions among acoustic phonons and low-frequency optical phonons. Moreover, with a sample size of 5 μm and 10 nm, the κ_{lat} is 25.4 W/mK and 11.4 W/mK at room temperature, respectively. Our results reveal that the κ_{lat} of novel 2D NP is significantly affected by sample length, which thus provides beneficial information for further studies on related materials.

2. Computational methods

All of the calculations are implemented in vasp code. We used PAW pseudopotentials with PBE exchange–correlation [13–15]. DFT-D2 type vdW method was adopted [16]. An MP k-mesh of 20 × 20 × 1 and 500 eV energy cutoff are selected during the calculation. The energy and force convergences are 10^{-9} eV and 10^{-4} eV/Å. The thickness is 20 Å, avoiding a fictional phenomenon.

The calculation of κ_{lat} is based on ShengBTE [17]. The second-order interatomic force constants (IFCs) were calculated by Phonopy [18]. We used 7 × 7 × 1 supercell and 3 × 3 × 1 k-mesh. For the 3rd IFCs, we used 4 × 4 × 1 supercell with 5 × 5 × 1 k-mesh. Fig. 1(a) and (b) show the convergence of κ_{lat} with different cutoff radii of third-order, scale broadening parameter, and q-point grid. The cutoff radius was increased until the converged results within 5% (thirteenth-nearest-neighbor). Besides, the scale broadening parameter and q-point grid were adopted as 1.0 and 100 × 100 × 1, separately. Furthermore, the non-analytic correction was also considered based on the Born effective charges and the dielectric constants.

3. Results and discussions

The equilibrium structure of novel 2D NP shows in Fig. 2(a). For comparison, Table 1 lists the optimized lattice constant, bond length, buckling distance, and cohesive energy for monolayer β-NP and phosphorene, which cater to previous literature results [9,19–22]. The N-P bond length of novel 2D NP is 1.78 Å and is smaller than that of buckled monolayer phosphorene of 2.25 Å on account of the stronger interactions between N and P atoms. Obviously, the cohesive energy of the novel 2D NP with 4.27 eV/atom is more than those of monolayer β-NP of 4.14 eV/atom and phosphorene of 3.51 eV/atom. Hence, the novel 2D NP is stable in energy, just as the monolayer β-NP and phosphorene.

Fig. 2(b) illustrates the calculated phonon dispersion along with high-symmetry points for novel 2D NP. It is clear that novel 2D NP is dynamically stabile owing to free of imaginary frequency. Besides, there is a kink around Γ point of ZA mode. This phenomenon is also shown in the PbSe monolayer with the same structure of novel 2D NP [10]. The kink is related to the electron–phonon interaction, which has also been confirmed by previous work [23–25]. Moreover, the novel 2D NP has a zero acoustic-optical (a-o) phonon gap, and the entanglement is between transverse acoustic (TA), longitudinal acoustic (LA) modes and low frequency optical (low-o) phonons. This may imply a strong a-o phonon scattering and a low lattice thermal conductivity κ_{lat}. For instance, PbSe and SnSe sheets with ultra-low κ_{lat} mainly stem from a-o phonon scattering [26]. Fig. 2(c) shows the calculated phonon partial densities of states (DOS) of novel 2D NP. The phonon DOS of acoustic phonon modes and low-o phonons are dominated by the vibrations of phosphorus (P) atoms, while the vibrations of nitrogen (N) atoms primarily contribute to the DOS of high frequency optical (high-o) phonons.

The vibrations of the x-y plane and out-plane direction (z) for the P and N atoms are presented in Fig. 3(a)-(d) according to the continuity of their eigenvectors [18,26,27], namely $\left|\sum e^{*}_{k,\sigma_1}(i)\cdot e_{k+\Delta,\sigma_2}(i)\right| = \left|\delta_{\sigma_1,\sigma_2} - o(\Delta)\right|$, in which $e^{*}_{k,\sigma_1}(i)$ and Δ denote the displacement of the atom i, respectively, and (k,σ) represents a phonon mode. It is found that the vibrations of P atoms and N atoms show a strong hybrid in the xy-plane, and also the vibrations in the out-plane (z). What's more, the low-o branches are dominated by the x-y plane vibrations of the P atoms and N atoms. Similarly, the out-plane direction (z) vibrations contribute most to the ZA acoustic phonon branch, while the TA and LA acoustic phonon branches are derived from the x-y plane vibration.

The lattice thermal conductivity κ_{lat} can be obtained by the formula [17]

$$k_{\alpha\beta} = \frac{1}{V}\sum_{\lambda,q} C_{\lambda,q}(v^{\alpha}_{\lambda,q})^2 \tau^{\alpha}_{\lambda,q}, \quad (1)$$

where V denotes the volume of the primitive cell, $C_{\lambda,q}$,$v^{\alpha}_{\lambda,q}$, and $\tau^{\alpha}_{\lambda,q}$ are the specific heat, phonon group velocity, and phonon lifetime with mode λ and wave vector q along the α direction, respectively. In the present study, the effective thickness h is adopted as 6.85 Å, which is the summation of d and van der Waals radii of the outmost surface N atom [28,29].

Fig. 4(a) displays the calculated κ_{lat} of novel 2D NP with the iterative approach and the single-mode relaxation time approximation (RTA) solution. At room temperature, the calculated κ_{lat} are 25.4 W/mK and 10.2 W/mK for the iterative approach and RTA solution, respectively. It is noteworthy that the RTA method generally underpredicts lattice thermal conductivity κ_{lat}, and the RTA method is particularly useful for quite big samples size and slow heating experimental conditions [30].

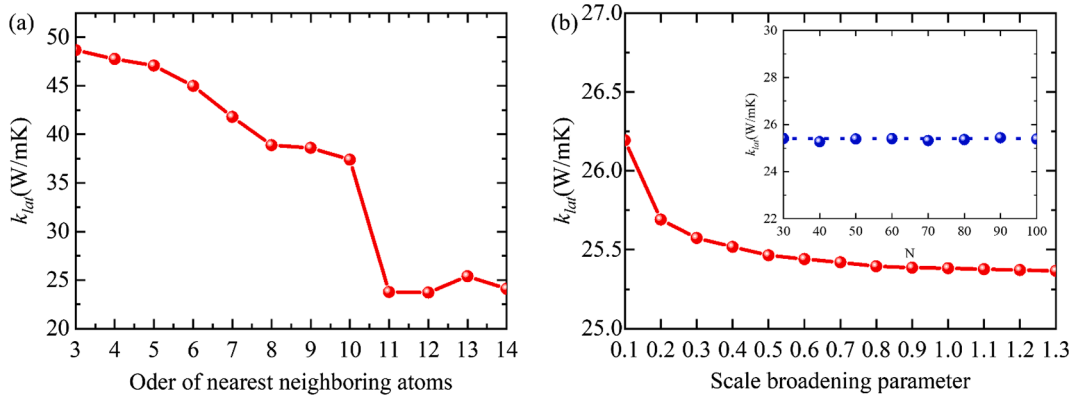

Fig. 1. The convergence test of κ_{lat} versus (a) cutoff radius of third-order IFCs, (b) different scale broad values, and q-point grid at room temperature for novel 2D NP.

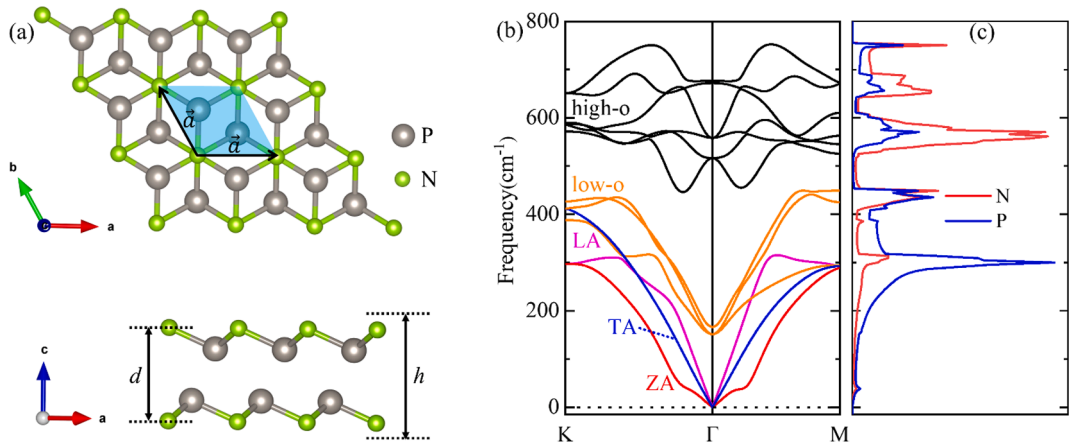

Fig. 2. (a) The top and side view of optimized structure, (b) phonon dispersion, and (c) phonon partial densities of states for novel 2D NP. In (a), the blue shading represents the unit cell, $\vec{a}$, d, and h are the lattice vectors, buckling distance, and effective thickness, respectively. (For interpretation of the references to colour in this figure legend, the reader is referred to the web version of this article.)

Table 1
The optimized lattice constant, bond length, buckling distance, and cohesive energy for novel 2D NP monolayer β-NP, monolayer phosphorene, and available literature.

materials	lattice constant (Å)	bond length (Å)	buckling distance (Å)	cohesive energy (eV/atom)
novel NP	2.82	1.78	3.27	4.27
β-NP	2.72,2.73[9] 2.756[20]	1.79, 1.809[20]	0.86, 0.86 [19], 0.86[20]	4.14, 4.086[20]
phosphorene	3.26, 3.28[9] , 3.28[21]	2.25, 2.26 [21]	1.24, 1.24 [21], 1.24[22]	3.51

Moreover, the Umklapp scattering dominates the heat transport of the novel 2D NP since the κ_{lat} can be nicely fitted by a function of $\kappa_{lat} \propto 1/T$. Interestingly, the κ_{lat} of novel 2D NP is lower than those of black phosphorene of 83.5 W/mK [31], graphene of 3716.6 W/mK [21], MoS_2 of 84 ± 17 W/mK [32], WSe_2 of 53 W/mK [33], buckled arsenene of 37.8 W/mK [12], phosphorene of 108.8 W/mK [11], nitrogene of 763.4 W/mK [12], β-NP of 572.3 W/K [9], β-NAs of 769.2 W/K [9] and β-NSb of 693.2 W/K [9]. Fig. 4(b) displays the frequency-dependent κ_{lat} at room temperature for novel 2D NP. It clearly shows that the κ_{lat} is dominated by those phonons below 450 cm^{-1}, which significantly contributes to the κ_{lat} from acoustic phonons and low-o phonons.

The calculated results of phonon group velocity V_g and phonon relaxation time τ at room temperature are shown in Fig. 5(a) and (b), separately. Based on the analysis of V_g and τ, we reveal reasonably that the phonon relaxation time τ is the main factor that significantly affects the thermal transport of novel 2D NP since the difference of group velocities is small. The calculated phonon velocities are presented in Fig. 5(a). The different distribution of phonon velocities results from the different shapes of phonon modes. Specifically, a small and nonzero sound velocity is observed in the ZA branch due to the linear component near Γ point, as dumbbell silicone [34]. Fig. 5(b) shows the phonon lifetime of phonon modes as a function of frequency. The domination of acoustic and low-optical phonons comes from their high value of τ, especially those phonons below 450 cm^{-1}, which is in an agreement with Fig. 4(b). Additionally, a strong acoustic-optical phonon scattering appears near the frequency of 250 cm^{-1} owing to a sharp drop of phonon relaxation time τ, and it can further suppress the κ_{lat} of novel 2D NP.

Fig. 5(c) shows the contribution (percentage) of phonon modes to the total κ_{lat} at room temperature. It is clearly seen that the ZA acoustic mode contributes a larger percentage compared with other phonon modes owing to the biggest phonon relaxation time τ, which has been verified in Fig. 5(b). Specifically, the contribution of low-optical phonon modes is non-negligible for the total κ_{lat}, and the percentage contributions are 33.07%, 18.67%, 14.49%, 30.69%, and 3.08% to the total intrinsic κ_{lat} for ZA, TA, LA, low-optical, and high-optical phonon modes, respectively.

The result of mode-dependent Grüneisen parameter γ for novel 2D NP is displayed in Fig. 5(d). The large γ means a stronger anharmonicity of phonons. It is clear that ZA and TA phonon modes possess a stronger anharmonicity compared with LA phonon mode below the frequencies of 150 cm^{-1}. Besides, γ suddenly jumps in the frequency range 150 cm^{-1} ~ 350 cm^{-1}, indicating a larger anharmonic scattering interaction change between the acoustic phonon modes and low-optical phonon modes. The result can also be confirmed in the phonon relaxation time shown in Fig. 5(b). The large γ of the low-o phonon modes

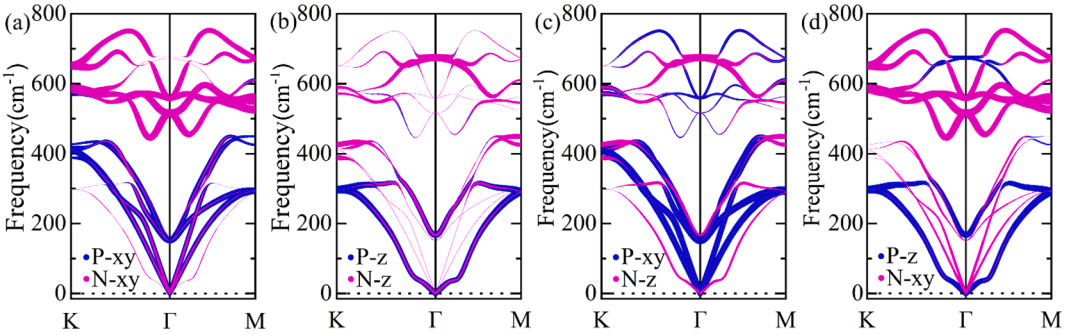

Fig. 3. (a)-(d) Orbital-resolved phonon spectra for novel 2D NP. The x-y plane and out-plane direction (z) vibrations of P and N atoms are represented by blue and magenta curves, respectively. (For interpretation of the references to colour in this figure legend, the reader is referred to the web version of this article.)

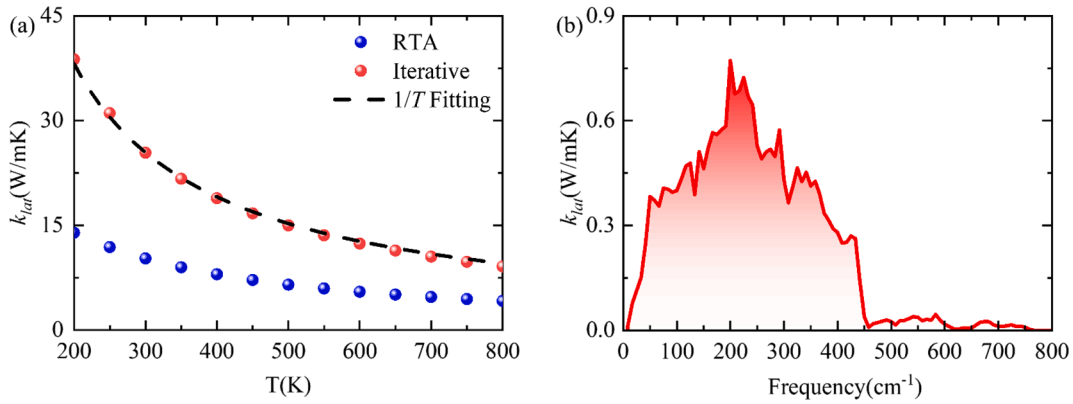

Fig. 4. (a) The variation *of* κ_{lat} with temperature for novel 2D NP. The temperature-dependent κ_{lat} is represented by the ~ 1/T fitting in the black dashed curve. (b) Frequency distribution of κ_{lat} at 300 K.

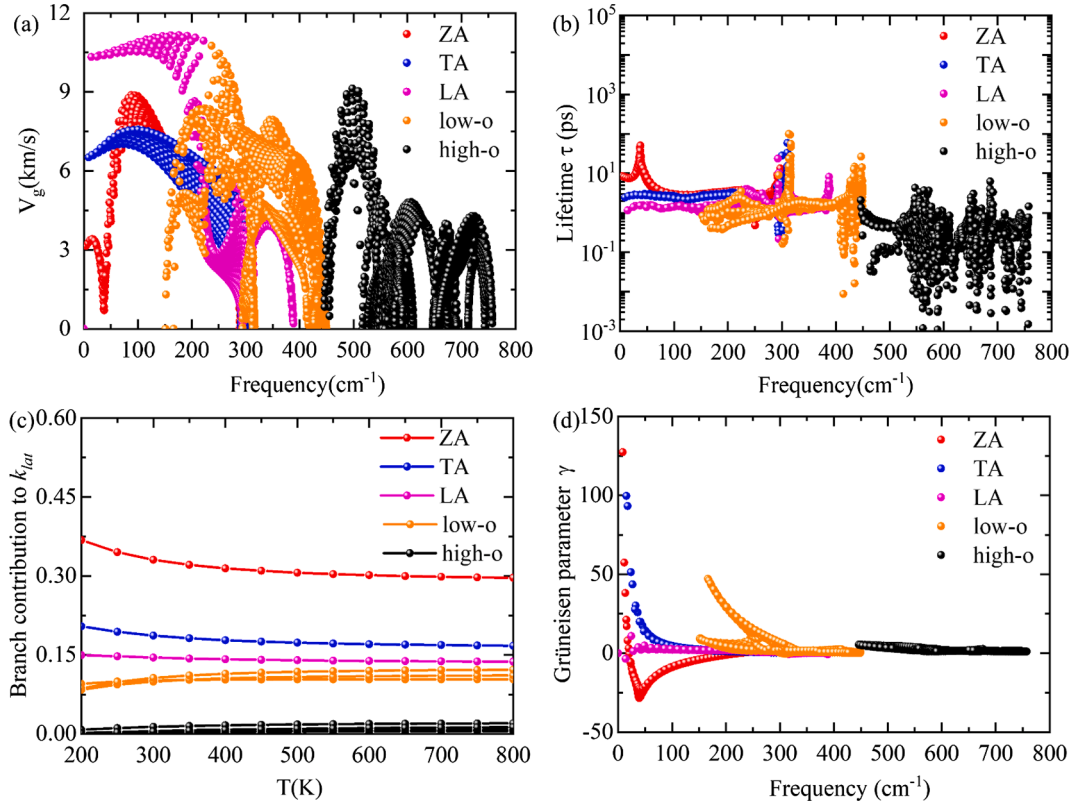

Fig. 5. (a) The phonon group velocity, (b)phonon lifetime, (c) relative contribution (percentage), and (d) Grüneisen parameters γ of phonon modes for novel 2D NP.

enhance the scattering rates and anharmonicity, leading to the low κ_{lat}.

To further explore the low intrinsic κ_{lat} in novel 2D NP. The three-phonon scattering phase space of the adsorption process ($P_3^{(+)}$) and emission process ($P_3^{(-)}$) are calculated and exhibited in Fig. 6(a) and (b), respectively. The absorption channels are dominated by ZA, TA, LA, and low-o phonon branches. Specifically, the low-o phonon branches display a large scattering phase space near 250 cm^{-1}. It is found that scattering interactions are strong among acoustic phonons and low-o phonons. The $P_3^{(-)}$ of novel 2D NP are mainly determined by optical phonon branches, as shown in Fig. 6(b). The result will enhance the number of o → a + a and o → a + o scattering channels.

To further describe the differences in anharmonic scattering, Fig. 6 (c) and (d) show the three-phonon scattering rates of absorption and emission processes. The acoustic and optical phonon branches are represented by "a" and "o", respectively. It is clear that the scattering rates of a + a → a scattering channel dominate in the frequency range below 150 cm^{-1}. Fig. 6(c) demonstrates the scattering rates of $P_3^{(+)}$, and it is predominated by a + a → o and a + o → o channels between 150 cm^{-1} and 450 cm^{-1}. It shows that an acoustic mode would more likely be scattered into an optical mode by absorbing an acoustic mode or an optical mode. The involvement of low-o mode increases the three-phonon scattering rate, which will bring about a further reduction of κ_{lat} in novel 2D NP. The emission process is presented in Fig. 6(d), the scattering rates of o → a + a and o → a + o channels illustrate that the optical phonon mode possesses more chance to decay into two acoustic modes or one acoustic mode and one optical mode. Those conclusions are consistent with the results of three-phonon scattering phase space for the adsorption process and emission process in Fig. 6(a) and (b).

In practical application, the sample size of the material is finite. The phonon-boundary scattering, at the nanoscale and low temperatures,

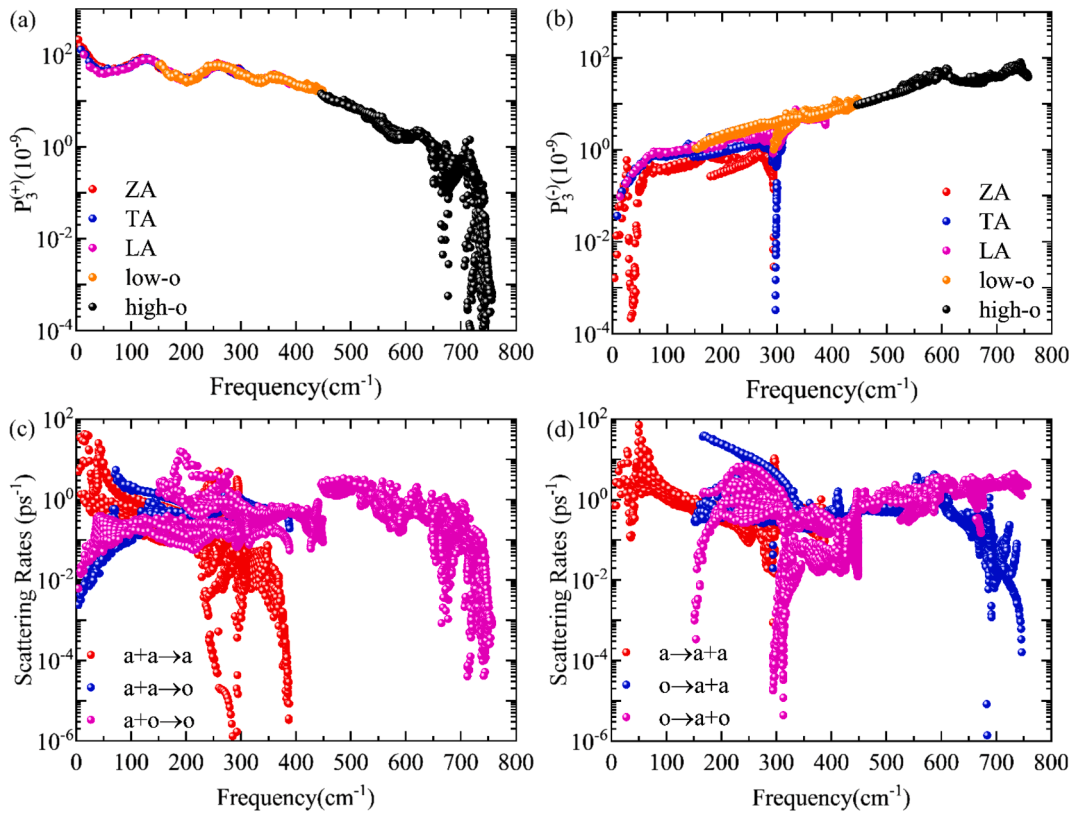

Fig. 6. Frequency-dependence of three-phonon-scattering phase space for (a) absorption, and (b) emission processes of novel 2D NP. The calculated scattering rates of (c) the absorption and (d) the emission processes for different phonon scattering channels.

significantly affects the transport properties of in 2D materials, and it has been well verified [35,36]. An inversely proportional relation exists between the phonon-boundary scattering and sample size L, given by [37–39]

$$\frac{1}{\tau_b} = \frac{|v_{vq}|}{L}, \tag{2}$$

where $\frac{1}{\tau_b}$ represent phonon-boundary scattering, L is the sample size as well as v_{vq} indicates averaged phonon group velocity. At different temperatures, the calculated size-dependent κ_{lat} of novel 2D NP is showed in Fig. 7(a). It exhibits an exponential function $\kappa_{lat} \propto \log L$ dependence between the κ_{lat} and sample size when L changes in the size range 100 nm ~ 10 nm. The result has been verified in the experiment for graphene and other 2D materials [40]. With a sample size of 5 μm and 10 nm, the κ_{lat} is 25.4 W/mK and 11.4 W/mK at 300 K, respectively. However, the κ_{lat} is independent of sample size L above 5 μm, which indicates that $L = 5$ μm reaches a boundary scattering limit. At 200 K and 500 K, a similar changing trend of the κ_{lat} can be also observed. For instance, at low temperatures, κ_{lat} decreases rapidly at 200 K on account of the significant effect of phonon-boundary scattering. Furthermore, the κ_{lat} is almost the same at different temperatures for a small sample size, which implies that κ_{lat} is dominated by phonon-boundary scattering up to a certain sample size.

The lattice thermal conductivity κ_{lat} changes with the temperature T for different sample sizes, which is displayed in Fig. 7(b) for novel 2D NP with different L. The κ_{lat} declines with reducing sample size because of the phonon-boundary scattering. For $L = 50$ nm, 100 nm, 500 nm, 1 μm, and 5 μm, κ_{lat} decreases rapidly with increasing temperature. This trend is also seen in the temperature range 200 K ~ 800 K for $L = \infty$. However,

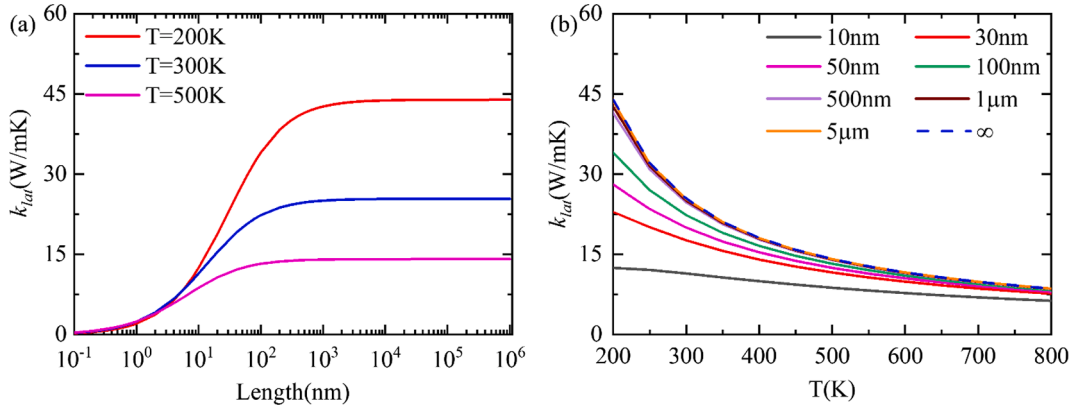

Fig. 7. (a) The variation of κ_{lat} with respect to sample size at $T = 200$ K, 300 K and 500 K. (b) The κ_{lat} variation with temperature for L = 10 nm, 30 nm, 50 nm, 100 nm, 500 nm, 1 μm, 5 μm and ∞ ($L = \infty$ refers to the case without phonon-boundary scattering).

κ_{lat} decreases slowly for a sample size of 10 nm. Our result demonstrates that κ_{lat} of novel 2D NP can be further reduced by decreasing the sample size. A similar phenomenon is also reported in our previous studies about novel monolayer CSe [41].

4. Conclusion

In summary, the phonon BTE is utilized to systematically explored the thermal transport properties of novel 2D NP. We have found that the κ_{lat} of novel 2D NP is 25.4 W/mK at room temperature, which is much lower than that of buckled monolayer phosphorene, nitrogene, β-NP, β-NAs, and β-NSb. We find the main influencing factor of κ_{lat} is phonon relaxation time through extensive analysis of the thermal transport properties. As a result, the ZA acoustic phonon branch contributes most compared with other phonon modes due to the large phonon relaxation time. The scattering rates of a + a ↔ o and a + o ↔ o channels show the strong scattering interactions among acoustic phonons and low-o phonons, which lead to further reduction of the κ_{lat} in novel 2D NP. At room temperature, with reducing the sample length L in the range 5 μm ~ 10 nm, the κ_{lat} can be further decreased from 25.4 W/mK to 11.4 W/mK. Moreover, the size effects of novel 2D NP can persist up to a length of 5 μm.

CRediT authorship contribution statement

Bing Lv: Writing - original draft, Software, Visualization. **Xiaona Hu:** Formal analysis, Visualization. **Ning Wang:** Writing - review & editing. **Jia Song:** Formal analysis, Visualization. **Xuefei Liu:** Visualization. **Zhibin Gao:** Writing - review & editing, Visualization.

Declaration of Competing Interest

The authors declare that they have no known competing financial interests or personal relationships that could have appeared to influence the work reported in this paper.

Acknowledgments

We thank Kunpeng Yuan for the helpful discussions. This work is supported by the National Natural Science Foundation of China (Grant No. 61564002 and 11664005), International Scientific and Technological Cooperation Projects of Guizhou Province, China (Grant No. [2013] 7019) and the State Key Laboratory for Mechanical Behavior of Materials. The authors would also like to thank Dr. X.D. Zhang and Mr. F. Yang at the Network Information Center of Xi'an Jiaotong University for support of the HPC platform.

References

[1] J.P. Heremans, M.S. Dresselhaus, L.E. Bell, D.T. Morelli, When thermoelectrics reached the nanoscale, Nat. Nanotechnol. 8 (2013) 471–473.
[2] L.D. Zhao, S.H. Lo, Y. Zhang, H. Sun, G. Tan, C. Uher, C. Wolverton, V.P. Dravid, M. G. Kanatzidis, Ultralow thermal conductivity and high thermoelectric figure of merit in SnSe crystals, Nature 508 (2014) 373–377.
[3] Z. Gao, F. Tao, J. Ren, Unusually low thermal conductivity of atomically thin 2D tellurium, Nanoscale 10 (2018) 12997–13003.
[4] Z. Gao, J.-S. Wang, Thermoelectric Penta-Silicene with a High Room-Temperature Figure of Merit, ACS Appl. Mater. Interfaces 12 (2020) 14298–14307.
[5] G.K.H. Madsen, D.J. Singh, BoltzTraP. A code for calculating band-structure dependent quantities, Comput. Phys. Commun. 175 (2006) 67–71.
[6] S.-D. Guo, J.-T. Liu, Lower lattice thermal conductivity in SbAs than As or Sb monolayers: a first-principles study, PCCP 19 (2017) 31982–31988.
[7] T. Kocabas, D. Cakir, O. Gulseren, F. Ay, N. Kosku Perkgoz, C. Sevik, A distinct correlation between the vibrational and thermal transport properties of group VA monolayer crystals, Nanoscale 10 (2018) 7803–7812.
[8] Y. Sun, Z. Shuai, D. Wang, Lattice thermal conductivity of monolayer AsP from first-principles molecular dynamics, Phys. Chem. Chem. Phys. 20 (2018) 14024–14030.
[9] A. Taheri, C. Da Silva, C.H. Amon, Phonon thermal transport in β− N X (X= P, As, Sb) monolayers: A first-principles study of the interplay between harmonic and anharmonic phonon properties, Phys. Rev. B 99 (2019), 235425.
[10] X.-L. Zhu, C.-H. Hou, P. Zhang, P.-F. Liu, G. Xie, B.-T. Wang, High Thermoelectric Performance of New Two-Dimensional IV–VI Compounds: A First-Principles Study, J. Phys. Chem. C 124 (2019) 1812–1819.
[11] G. Zheng, Y. Jia, S. Gao, S.-H. Ke, Comparative study of thermal properties of group-VA monolayers with buckled and puckered honeycomb structures, Phys. Rev. B 94 (2016), 155448.
[12] B. Peng, H. Zhang, H. Shao, Y. Xu, G. Ni, R. Zhang, H. Zhu, Phonon transport properties of two-dimensional group-IV materials from ab initio calculations, Phys. Rev. B 94 (2016), 245420.
[13] G. Kresse, J. Furthmüller, Efficiency of ab-initio total energy calculations for metals and semiconductors using a plane-wave basis set, Comput. Mater. Sci. 6 (1996) 15–50.
[14] G. Kresse, J. Furthmüller, Efficient iterative schemes for ab initio total-energy calculations using a plane-wave basis set, Phys. Rev. B 54 (1996) 11169.
[15] G. Kresse, D. Joubert, From ultrasoft pseudopotentials to the projector augmented-wave method, Phys. Rev. b 59 (1999) 1758.
[16] S. Grimme, Semiempirical GGA-type density functional constructed with a long-range dispersion correction, J. Comput. Chem. 27 (2006) 1787–1799.
[17] W. Li, J. Carrete, N.A. Katcho, N. Mingo, ShengBTE: A solver of the Boltzmann transport equation for phonons, Comput. Phys. Commun. 185 (2014) 1747–1758.
[18] A. Togo, I. Tanaka, First principles phonon calculations in materials science, Scr. Mater. 108 (2015) 1–5.
[19] J. Lee, W.-C. Tian, W.-L. Wang, D.-X. Yao, Two-dimensional pnictogen honeycomb lattice: structure, on-site spin-orbit coupling and spin polarization, Sci. Rep. 5 (2015) 1–16.
[20] S. Ma, C. He, L.Z. Sun, H. Lin, Y. Li, K.W. Zhang, Stability of two-dimensional PN monolayer sheets and their electronic properties, PCCP 17 (2015) 32009–32015.
[21] B. Peng, D. Zhang, H. Zhang, H. Shao, G. Ni, Y. Zhu, H. Zhu, The conflicting role of buckled structure in phonon transport of 2D group-IV and group-V materials, Nanoscale 9 (2017) 7397–7407.
[22] H. Yin, J. Gao, G.-P. Zheng, Y. Wang, Y. Ma, Giant Piezoelectric Effects in Monolayer Group-V Binary Compounds with Honeycomb Phases: A First-Principles Prediction, J. Phys. Chem. C 121 (2017) 25576–25584.
[23] F. Giustino, M.L. Cohen, S.G. Louie, Small phonon contribution to the photoemission kink in the copper oxide superconductors, Nature 452 (2008) 975–978.
[24] A. Lanzara, P.V. Bogdanov, X.J. Zhou, S.A. Kellar, D.L. Feng, E.D. Lu, T. Yoshida, H. Eisaki, A. Fujimori, K. Kishio, Evidence for ubiquitous strong electron–phonon coupling in high-temperature superconductors, Nature 412 (2001) 510–514.
[25] D. Reznik, G. Sangiovanni, O. Gunnarsson, T.P. Devereaux, Photoemission kinks and phonons in cuprates, Nature 455 (2008) E6–E7.
[26] P.-F. Liu, T. Bo, J. Xu, W. Yin, J. Zhang, F. Wang, O. Eriksson, B.-T. Wang, First-principles calculations of the ultralow thermal conductivity in two-dimensional group-IV selenides, Phys. Rev. B 98 (2018), 235426.
[27] L.F. Huang, P.L. Gong, Z. Zeng, Correlation between structure, phonon spectra, thermal expansion, and thermomechanics of single-layer MoS 2, Phys. Rev. B 90 (2014), 045409.
[28] S.S. Batsanov, Van der Waals radii of elements, Inorg. Mater. 37 (2001) 871–885.
[29] Z. Gao, X. Dong, N. Li, J. Ren, Novel two-dimensional silicon dioxide with in-plane negative Poisson's ratio, Nano Lett. 17 (2017) 772–777.
[30] P. Torres, F.X. Alvarez, X. Cartoixà, R. Rurali, Thermal conductivity and phonon hydrodynamics in transition metal dichalcogenides from first-principles, 2D Materials 6 (2019), 035002.
[31] L. Zhu, G. Zhang, B. Li, Coexistence of size-dependent and size-independent thermal conductivities in phosphorene, Phys. Rev. B 90 (2014), 214302.
[32] X. Zhang, D. Sun, Y. Li, G.-H. Lee, X. Cui, D. Chenet, Y. You, T.F. Heinz, J.C. Hone, Measurement of lateral and interfacial thermal conductivity of single-and bilayer MoS_2 and $MoSe_2$ using refined optothermal Raman technique, ACS Appl. Mater. Interfaces 7 (2015) 25923–25929.
[33] X. Gu, R. Yang, Phonon transport in single-layer transition metal dichalcogenides: A first-principles study, Appl. Phys. Lett. 105 (2014), 131903.
[34] B. Peng, H. Zhang, H. Shao, Y. Xu, R. Zhang, H. Lu, D.W. Zhang, H. Zhu, First-principles prediction of ultralow lattice thermal conductivity of dumbbell silicene: a comparison with low-buckled silicene, ACS Appl. Mater. Interfaces 8 (2016) 20977–20985.
[35] A.A. Balandin, S. Ghosh, W. Bao, I. Calizo, D. Teweldebrhan, F. Miao, C.N. Lau, Superior thermal conductivity of single-layer graphene, Nano Lett. 8 (2008) 902–907.
[36] D.L. Nika, E.P. Pokatilov, A.S. Askerov, A.A. Balandin, Phonon thermal conduction in graphene: Role of Umklapp and edge roughness scattering, Phys. Rev. B 79 (2009), 155413.
[37] Z. Rashid, A.S. Nissimagoudar, W. Li, Phonon transport and thermoelectric properties of semiconducting Bi_2Te_2X (X = S, Se, Te) monolayers, PCCP 21 (2019) 5679–5688.
[38] L. Zhu, T. Zhang, Z. Sun, J. Li, G. Chen, S.A. Yang, Thermal conductivity of biaxial-strained MoS_2: sensitive strain dependence and size dependent reduction rate, Nanotechnology 26 (2015), 465707.
[39] Z. Gao, Z. Zhang, G. Liu, J.-S. Wang, Ultra-low lattice thermal conductivity of monolayer penta-silicene and penta-germanene, PCCP 21 (2019) 26033–26040.
[40] X. Xu, L.F.C. Pereira, Y. Wang, J. Wu, K. Zhang, X. Zhao, S. Bae, C.T. Bui, R. Xie, J. T.L. Thong, Length-dependent thermal conductivity in suspended single-layer graphene, Nat. Commun. 5 (2014) 1–6.
[41] B. Lv, X. Hu, X. Liu, Z. Zhang, J. Song, Z. Luo, Z. Gao, Thermal transport properties of novel two-dimensional CSe, PCCP 22 (2020) 17833–17841.